

Identifying Microplastics in Laboratory and Atmospheric Aerosol Mixtures via Optical Photothermal Infrared and Raman Microspectroscopy

Rebecca L. Parham, Abbygail M. Ayala, Lauren Meagher, Madeline E. Clough, Eduardo Ochoa Rivera, Jia H. Shi, Ambuj Tewari, Anne J. McNeil, and Andrew P. Ault*



Cite This: *Anal. Chem.* 2025, 97, 18136–18143



Read Online

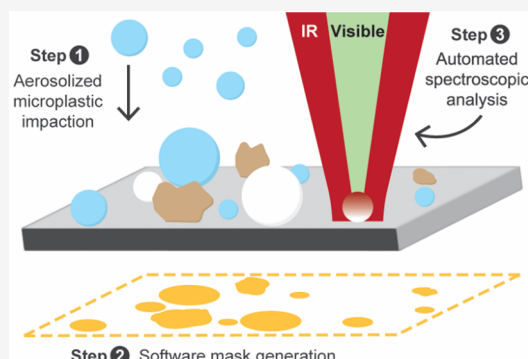
ACCESS |

Metrics & More

Article Recommendations

Supporting Information

ABSTRACT: The widespread release of plastic waste into the environment, combined with its chemical stability, has resulted in microplastics (MPs) being observed in diverse locations, ranging from urban centers to remote areas. However, the impacts of MPs on human health, ecosystems, and the climate are still being discovered. Infrared (IR) microscopy is widely used to identify MPs in water and soil samples, but it struggles to measure atmospheric MPs due to their smaller size and the diffraction limit of IR radiation. Herein, optical photothermal IR coupled with Raman (O-PTIR+Raman) microspectroscopy is used to classify MPs by polymer type at atmospherically relevant sizes ($\leq 10 \mu\text{m}$). Detecting changes in elastic scattering of visible photons after IR absorption and photothermal expansion improves O-PTIR spatial resolution and enables analysis of particles with diameters $\geq \sim 0.8 \mu\text{m}$. A recently developed computer-controlled (CC) particle analysis module was used, which decreased analysis time by at least 30%. O-PTIR and Raman independently identified and distinguished high-density polyethylene (HDPE), polypropylene (PP), and polystyrene (PS) within the same sample and within samples containing particles generated with atmospherically relevant standards (ammonium sulfate, sodium nitrate, and sucrose). CC-O-PTIR+Raman was also able to distinguish MPs impacted onto an already collected sample of ambient atmospheric particles. All three samples (MPs-Only, MPs+Standards, and MPs+Ambient) were comprised of particles $\leq 10 \mu\text{m}$. Our results demonstrate how CC-O-PTIR+Raman can expand capabilities for MP identification to cover atmospherically-sized particles and reduce analysis time, thereby improving understanding of atmospheric MP exposure and potential impacts on human health and the environment.



INTRODUCTION

Since the 1950s, plastic production has increased rapidly, most of which ends up in landfills or the environment.^{1,2} Moreover, mismanaged plastic waste can break down into microplastics (MPs), which are plastic particles between 1–5000 μm in diameter.³ The initial focus of environmental MP research was on aquatic and terrestrial environments⁴ until 2015, when the atmospheric deposition of MPs was first observed by Dris et al.⁵ in Paris, France. There have since been numerous reports of atmospheric MPs in megacities,^{6–11} protected nature areas,¹² and remote regions,^{13–17} with the differences in reported deposition rates and concentrations varying widely. However, these results are difficult to compare due to the lack of standardization in sample collection, processing, and analysis methods.^{18–21}

Evidence of human exposure to atmospheric MPs has also been increasing. Recently, MPs have been measured in lung tissue samples from adults.^{22,23} Research is still limited on the toxicological and epidemiological implications of inhaling MPs, making it difficult to determine the overall risks to human health.²⁴ Particulate matter $\leq 10 \mu\text{m}$ (PM_{10}) and $\leq 2.5 \mu\text{m}$

($\text{PM}_{2.5}$) are regulated by the U.S. Environmental Protection Agency (EPA), as particles in these size ranges (especially $\text{PM}_{2.5}$) have sufficient atmospheric lifetimes to present an inhalation risk, penetrate deeply into the lungs, and are associated with a range of negative health effects.^{25–29} A critical objective for future atmospheric MP research includes collecting more data on exposure to MP particles $\leq 10 \mu\text{m}$, as there is little information on their concentrations in the atmosphere and in these size ranges.^{20,21,24}

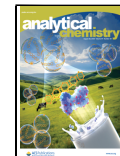
Identifying MPs in the complex milieu of the environment requires methods that can differentiate synthetic polymers from naturally occurring organic and inorganic materials on a particle-by-particle basis. Vibrational spectroscopies (e.g.,

Received: May 17, 2025

Revised: July 21, 2025

Accepted: August 5, 2025

Published: August 14, 2025



infrared (IR) and Raman) can identify specific functional groups and patterns from polymers that can be compared against extensive commercial IR and Raman spectral libraries to determine MP polymer types.^{30,31} Popular IR techniques for MP analysis include microattenuated total reflection Fourier transform infrared (μ -ATR-FTIR) spectroscopy and μ -FTIR with a focal plane array (FPA) detector and quantum cascade laser (QCL).^{32,33} However, these methods struggle to collect spectra from real-world MPs $< \sim 20 \mu\text{m}$ in diameter due to the diffraction limit of IR radiation,^{11,12,30–32,34} meaning that μ -FTIR techniques largely miss MPs $\leq 10 \mu\text{m}$ despite evidence that a large number of MPs are in these smaller size ranges.^{13,16,20} Raman microspectroscopy, in contrast, is able to detect MPs $< 1 \mu\text{m}$ as visible light can be focused to a greater extent than longer-wavelength IR photons.^{13,35,36} For example, Käppler et al.³¹ reported that μ -FTIR underestimated the number of MP particles $< 20 \mu\text{m}$ by almost 35% when compared with Raman microspectroscopy. However, Raman is frequently overwhelmed by fluorescence, which is prevalent in environmental samples,^{37,38} limiting the range of samples that can be analyzed. A common recommendation for identifying atmospheric MPs in complex matrices has been to use both μ -FTIR and μ -Raman instruments to overcome their respective limitations.^{31,34,39}

Optical photothermal infrared (O-PTIR) spectroscopy, which is part of the class of PTIR techniques, has been established as an indirect IR analysis method for particles $< 1 \mu\text{m}$, where a visible laser probes the photothermal response of a particle (e.g., increased size and shift in refractive index) to a tunable IR laser source.⁴⁰ Given that the peak locations and relative peak intensities of plastic spectra obtained from O-PTIR can be slightly different from those obtained from traditional IR techniques,³⁹ these spectra will herein be referred to as “PTIR” spectra to distinguish them from traditional Beer’s Law-based IR spectra. By monitoring elastic scattering from the visible laser, O-PTIR can achieve the same submicron spatial resolution as Raman microspectroscopy.⁴⁰ Moreover, inelastically scattered photons (specifically Stokes-shifted photons) can be directed to a Raman spectrometer—thus allowing for simultaneous single-particle PTIR and Raman spectroscopic measurements.⁴¹ Measuring both PTIR and Raman also improves the confidence when identifying a particle as an MP.³⁹

A significant drawback of O-PTIR+Raman to date has been its lack of automated particle-by-particle analysis, causing the technique to be time and labor-intensive.³⁰ Herein, we demonstrate computer-controlled O-PTIR+Raman (CC-O-PTIR+Raman) can automatically detect and analyze particles in a field of view (FOV), increasing throughput and reducing human-guided selection biases. The capabilities of this module are demonstrated by identifying and quantifying individual MPs in particle mixtures of increasing complexity, including a mixture of MPs, MPs mixed with particles of proxy atmospheric aerosols, and MPs added onto to an already collected real-world atmospheric particle sample. Using CC-O-PTIR+Raman to measure atmospheric MPs will enable improved identification of MPs in ambient samples, advancing our understanding of atmospheric MP concentrations and associated inhalation exposure risks.

■ EXPERIMENTAL SECTION

Laboratory-Generated Aerosol Particle Samples.

Suspensions and solutions were prepared using dry high-

density polyethylene spheres (HDPE, 0.2–9.9 μm , Cospheric), polypropylene powder (PP, 1–5 μm , 99% purity, Nanochemazone, Canada), two sizes of polystyrene latex spheres (PS, 1.75 and 2.50 μm , NIST traceable, Polysciences, Inc.), ammonium sulfate (AS, $\geq 99.0\%$ purity, Sigma-Aldrich), sodium nitrate (SN, $\geq 99.0\%$ purity, Sigma-Aldrich), D-sucrose (SCR, $\geq 99.9\%$ purity, Fisher Scientific), and ethanol ($\geq 99.5\%$ purity, Thermo Scientific Chemicals, Canada). All materials were suspended or dissolved in 18.2 MΩ·cm Milli-Q water, except for the HDPE and PP powders. HDPE and PP powders, specifically, were prepared in cold 50/50 ethanol/Milli-Q (v/v), sonicated for 3 min in an ice bath, and immediately aerosolized to mitigate particle aggregation at the surface of the suspension. The PS suspension was also sonicated for 10 min before use.

All suspensions and solutions were aerosolized with nitrogen gas (filtered through a high efficiency particulate arrestance (HEPA) filter) and a Collison nebulizer, flowed through a diffusion dryer, and impacted onto silicon wafers with a 100 nm thick aluminum coating (Platypus Technologies) on stage 2 (0.4–2.8 μm aerodynamic diameter, d_a) of a Microanalysis Particle Sampler (MPS, California Measurements, Inc.). A sample containing only MPs, referred to as “MPs-Only”, was made by sequentially impacting HDPE, PP, and PS particles. A second sample containing MPs and particles generated from atmospheric proxies, called “MPs+Standards”, was made by sequentially impacting three MP and three non-MP (e.g., AS, SN, and SCR) particle types onto the same substrate. The number size distribution of particles aerosolized from each solution was measured by an Aerodynamic Particle Sizer (APS, TSI Incorporated, Figure S1), which measures size-resolved number concentrations from $d_a \sim 0.5\text{--}19 \mu\text{m}$. All samples were stored in the dark at room temperature following the recommended procedures in Laskina et al.⁴²

Computer-Controlled Optical Photothermal Infrared Coupled with Raman (CC-O-PTIR+Raman) Microspectroscopy. For CC-O-PTIR+Raman analysis, a mIRage instrument (Photothermal Spectroscopy Corp.) was used to analyze all samples. The mIRage setup included a confocal microscope equipped with a 20 \times objective (0.45 N.A., 6.90 mm working distance, Nikon), as well as a 40 \times Cassegrain objective (0.78 N.A., 8.3 mm working distance, Thor Laboratories) that focuses IR and visible light. A 532 nm continuous wave laser (200 mW power) was used as a probe, and a dual-range mIRcat-QT tunable QCL (120 mW maximum power, 10% duty cycle, 100 kHz pulse rate, 500 nm pulse width) scanned through frequencies to elicit photothermal response from the particle. The range of the mIRcat-QT was 948–1860 and 2698–3002 cm^{-1} split between four QCL chips (945–1230, 1115–1499, 1441–1866, and 2645–3012 cm^{-1}) with a spectral resolution of 2 cm^{-1} . Each PTIR spectrum was collected with 20% IR power, 5% probe power, and 10 averaged scans. The Raman spectra were collected over a range of 480–3762 cm^{-1} , with a slightly extended range on some runs, with a grating of 600 groove/mm and a spectral resolution of $\sim 3 \text{ cm}^{-1}$. Additional parameters for each Raman spectrum collected included a 15 s delay time (i.e., the amount of time the particle was exposed to the visible laser beam before collecting a Raman spectrum to help mitigate autofluorescence) and 3 \times 30 s averaged scans. Raman spectra were calibrated manually using the 520 cm^{-1} peak,³⁷ collected daily from a piece of silicon wafer, as well as the ambient gaseous nitrogen peak located at 2330 cm^{-1} .⁴³ All

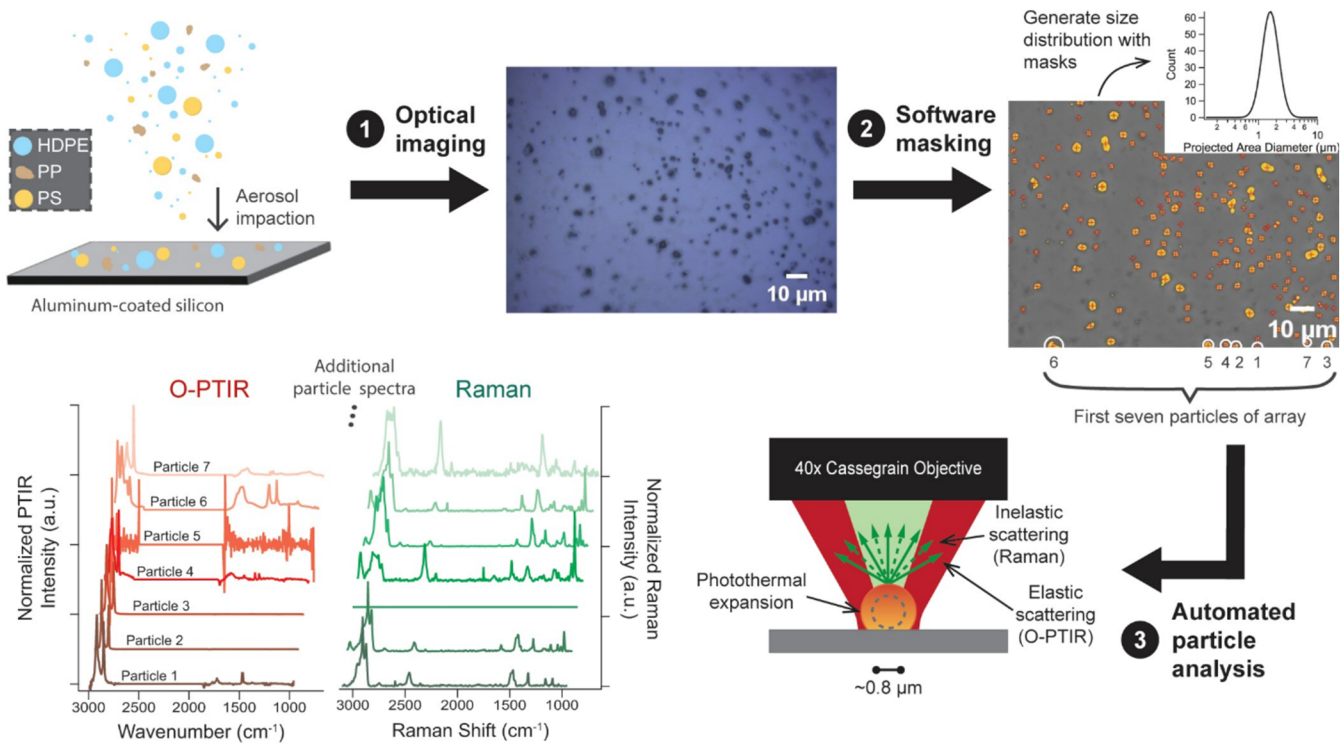


Figure 1. Schematic showing aerosol impaction, optical imaging (1), software masking (2), and automated particle analysis using O-PTIR+Raman (3). Particles were selected via contrast differences between the particles and the substrate/solvent residues as well as particle size ($\geq 0.5 \mu\text{m}$ projected area diameter), and a fitted size distribution was generated using the particles' masks (shown in yellow). Only the first seven particles are listed on the particle mask image and example O-PTIR+Raman spectra for simplicity.

PTIR and Raman spectra shown were normalized to their most intense peak. Additionally, Raman spectra were baseline corrected in PTIR Studios (baseline removal strength: 20).

Spectral collection with the mIRage was automated using the featurefindIR module in PTIR Studios (Photothermal Spectroscopy Corp., Figure S2). The module selects particles from one FOV with user-controlled settings such as contrast difference between particles and background, as well as particle size (Figure 1). In this study, the contrast parameters were varied to maximize individual particle detection without introducing false particles, and particles $\geq 0.5 \mu\text{m}$ projected area diameter (d_{pa}) were analyzed to push the lower bound of particle detection. PTIR and Raman spectra were then collected for the chosen array of particles.

Ambient Aerosol Sample. To test the capacity of CC-O-PTIR+Raman to identify MPs within complex atmospheric samples, ambient aerosol particle samples were collected for 3 h 45 min in Ann Arbor, Michigan, on May 1, 2024, on stage 2 of the MPS on a gridded silicon substrate (Ted Pella, Inc.). Ambient aerosol size distributions were collected with the APS (Figure S1). The impacted sample was analyzed with both CC-O-PTIR+Raman and CC-Raman (on a separate instrument),^{37,44} in a selected cell of the gridded substrate and manually analyzed for any MPs present. Out of the 262 particles analyzed with CC-O-PTIR+Raman, none of them were MPs. HDPE, PP, and PS were subsequently impacted onto the same area of the substrate as the ambient particles, and that area was reanalyzed with CC-O-PTIR+Raman and CC-Raman. The sample pre- and postimpaction of MPs is referred to as "Ambient-Only" and "MPs+Ambient", respectively, and an optical comparison can be seen in Figure S3.

Side-by-side results from CC-O-PTIR+Raman and CC-Raman can be found in Figure S4 and Tables S1–S3.

Particle Identification. An in-house reference library was generated to identify MP particles in the samples. Each of the six particle types (HDPE, PP, PS, AS, SN, and SCR) were aerosolized and impacted onto separate aluminum-coated silicon substrates using the setup previously described. A minimum of 20 particles were collected for each particle type. The spectra were then manually screened to remove those with too low of signal-to-noise ratios to identify peaks, and the remaining spectra were averaged for easier reference while manually identifying particles. The average reference spectra, herein referred to as only "reference spectra" for simplicity, as the mIRage O-PTIR+Raman libraries can be found in Figure S5 with their identifying modes listed in Table S4. All PTIR and Raman spectra from the MPs-Only, MPs+Standards, and MPs+Ambient samples were then manually labeled using the reference library for identification.

RESULTS AND DISCUSSION

To establish the capability of CC-O-PTIR+Raman to distinguish MPs within a sample, MP particles $< 5 \mu\text{m}$ in diameter were analyzed (Figure 2a) whose molecular structures are shown in Figure 2b. There were no commercial standards for fibers available at the time of this study, but it is expected that CC-O-PTIR+Raman could be applied to fibers given its similar optical setup with other microspectroscopic techniques and its documented capabilities to identify particles with diverse morphologies (e.g., cyanobacteria filaments⁴⁵). For the selected MP types, the PTIR and Raman spectra from individual particles compared with their corresponding spectra from the in-house reference library are shown in Figure 2c,d,

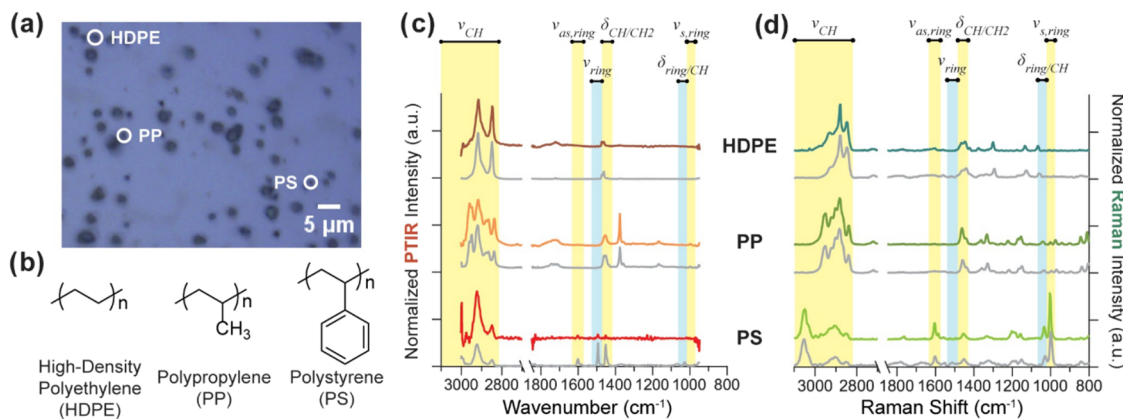


Figure 2. (a) Optical image of the MPs-Only sample, (b) chemical structures of MPs used, (c) PTIR spectra, and (d) Raman spectra from three example MP particles (identified in the image). Red/orange spectra (PTIR) and green spectra (Raman) are shown above a reference spectrum (gray) that was also generated for each MP type.

respectively. Obtaining both PTIR and Raman spectra for each particle, rather than collection of only one of the spectra at a time, improves the identification of MP particles in the MPs-Only sample. For example, the PTIR spectra for the HDPE and PS particles both have two prominent C–H stretches (ν_{CH}), where the former has peaks at 2848 and 2918 cm⁻¹ and the latter has peaks at 2848 and 2924 cm⁻¹.⁴⁶ The PTIR spectrum in the reference library for PS further exhibits a CH₂ bend ($\delta_{\text{CH/CH}_2}$) at 1462 cm⁻¹ as well as aromatic ring stretches (ν_{ring} and $\nu_{\text{as,ring}}$) at 1472 and 1602 cm⁻¹, respectively. However, the corresponding peaks in the spectrum of the example PS particle are lower in intensity, making it difficult to identify the particle as PS based on its PTIR spectrum alone.

When the Raman spectrum is also taken into consideration, HDPE and PS can be confidently distinguished based on the PS peaks at 1000 and 1031 cm⁻¹ for the symmetric ring stretch ($\nu_{\text{s,ring}}$) and in-plane ring deformation ($\delta_{\text{ring/CH}}$),⁴⁷ respectively, as well as 1604 cm⁻¹ for the antisymmetric ring stretch ($\nu_{\text{as,ring}}$ a.k.a. ring skeletal stretch),^{47,48} showing the value of Raman for PS chemical identification. The three MPs can be further distinguished from each other with Raman by their distinct C–H stretching regions (i.e., 2750–3000 cm⁻¹). HDPE has a defined peak at 2878 cm⁻¹ for the antisymmetric CH₂ stretch bordered by two peaks at 2847 and 2930 cm⁻¹ for symmetric CH₂ stretches. PP has a cluster of sharp peaks, with modes for the CH₂ symmetric stretch, C–H symmetric stretch, and CH₃ antisymmetric stretch at 2840, 2881, and 2951 cm⁻¹, respectively. Finally, PS has symmetric and antisymmetric CH₂ stretches at 2850 and 2906 cm⁻¹, respectively, and a sharp peak at 3051 cm⁻¹ for the C–H stretch. Cross-comparing the existence, or absence, of key peaks in the PTIR and Raman spectra for each particle is a valuable asset for correctly identifying particles.

O-PTIR+Raman already decreases data collection time for a user by obtaining two sets of spectra at the same time. However, automating the analysis makes data collection even more efficient. It generally takes 1.25–2 h to analyze 20 particles manually, depending on the expertise of the user with the instrument, whereas an automated approach reduces this time to 50 min. Similar observations have been reported for the difference between manual and automated analysis with Raman microspectroscopy.³⁷ It should also be noted that, in lieu of spectral collection, manually grouping spectra became the new bottleneck in the data analysis pipeline.

The improved efficiency of spectral collection makes it easier to collect larger data sets for quantitative analysis of a particle population. Figure 3a shows the fractions of each MP particle type, distinguished with blue hues, for the MPs-Only sample. Additionally, the particle type fractions between the PTIR and Raman classifications can be compared. The fractions of HDPE and PP had good agreement, with the HDPE fractions being well within the uncertainty of each other (PTIR: 0.25 ± 0.04, Raman: 0.24 ± 0.04) and the PP fractions both being 0.19 ± 0.03. A lower fraction of PS was observed with the O-PTIR (0.06 ± 0.02) versus Raman (0.17 ± 0.03), as the O-PTIR did not detect some particles that Raman did. These PTIR spectra were instead assigned to the LOW category (Table S1) since no peaks were distinguished from the background. Many particles <1.0 μm also ended up in the LOW category (Figure S6), as the signal decreased with decreasing particle size and the lowest detected size was ~550 nm. When compared with a standalone Raman system, the fraction of particles in the LOW category was within the range of uncertainty for the mIRage Raman and the standalone Raman (Figure S4 and Table S1). The MIX category was used to label spectra that had clear characteristic peaks of two or more particle types (e.g., HDPE and PP), which occasionally occurred when multiple particles were impacted on top of one another. The fractions of PTIR and Raman spectra in the MIX category were within uncertainty of each other. A final category called unsorted (UNS) was used to label spectra that either (1) had signal but could not be identified due to a lack of characteristic peaks or (2) were dominated by fluorescence or saturation of the detector (specifically for Raman spectra).

The MPs+Standards sample (Figure 3b) demonstrates that CC-O-PTIR+Raman can clearly distinguish between the MP particle types and the atmospheric-proxy particles generated from AS, SN, and SCR. The standards chosen include key components present in atmospheric aerosols. Sulfate and ammonium are present in a high fraction of atmospheric particles due to secondary formation processes (including SO₂ oxidation and NH₃ partitioning).⁴⁹ Sodium and nitrate are widely present in sea spray aerosol (SSA) after uptake of HNO₃ from NO_x oxidation.⁵⁰ Sucrose is a proxy for oxidized organic aerosol that forms from oxidation of volatile organic compounds (VOCs),⁵¹ and it was chosen as a carbonaceous proxy because another common method for MP analysis (CC-scanning electron microscopy with energy dispersive X-ray

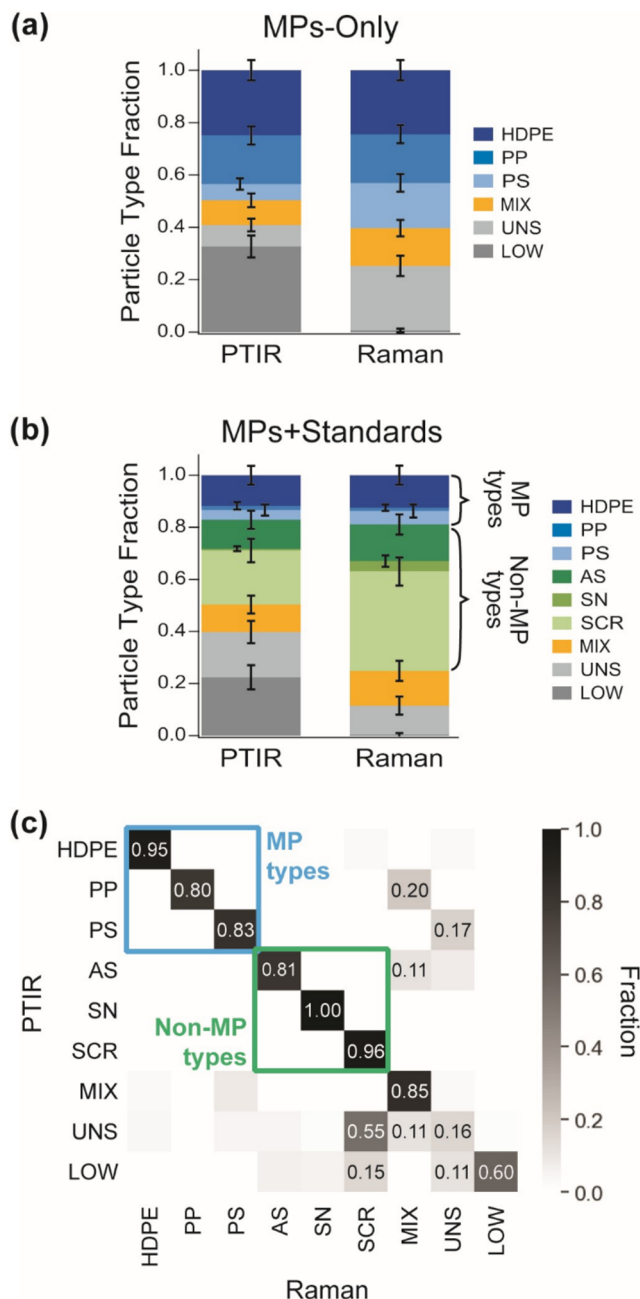


Figure 3. Particle fractions from labeled PTIR and Raman spectra for (a) MP-Only sample (particle count = 499) and (b) MP+Standards sample (particle count = 322). Error bars represent standard error for its respective particle type fraction. (c) Heat map of fractions between the sorted PTIR and Raman spectra for the MP+Standards sample (particle count = 429), with match fractions >0.10 labeled on their corresponding cells. MP and non-MP cells are boxed in blue and green, respectively, for clarity. Category labels are high-density polyethylene (HDPE), polypropylene (PP), polystyrene (PS), ammonium sulfate (AS), sodium nitrate (SN), and sucrose (SCR), mixture (MIX), unsorted (UNS), and low signal (LOW).

spectroscopy, CC-SEM-EDX)^{49,52,53} only provides elemental information, making it challenging to differentiate carbon-dominant particles from MPs.⁵⁴ The PTIR and Raman fractions of MP and non-MP particles were mostly within uncertainty of each other (Figure 3b). The exception was sucrose, which had a PTIR fraction of 0.11 ± 0.03 and a Raman fraction of 0.38 ± 0.05 (Table S2). Similarly to the PS

category in Figure 3a, this discrepancy is due to the number of PTIR spectra labeled as LOW compared to its Raman counterpart.

Simultaneously collecting two types of spectral information for each particle enables an even more comprehensive comparison between the techniques (Figure 3c). For example, the cell where the SCR labels for PTIR and Raman intersect has a match fraction of 96%—meaning that nearly all particles that had their PTIR spectra labeled as SCR also had their Raman spectra labeled as SCR. More information on the calculations used for the matrix can be found in Figure S7 and eq S1. The matrix shows strong agreement between the PTIR and Raman spectra for the same particles, as the match fractions exceed 80% along the diagonal line where the PTIR and Raman spectral labels are the same. MP and non-MP particle types are clearly distinguished (blue and green boxes, Figure 3c, respectively), and the same particles are identified as MIX with both O-PTIR and Raman. There are only a few cells with a match fraction >10% outside of these matching particle types, primarily for LOW, UNS, or MIX. Taken together, these samples show CC-O-PTIR+Raman clearly detects MPs $\leq 10 \mu\text{m}$ and differentiates the MPs from other non-MP particles as well as each other, thus extending the size range that can be probed by IR into an underrepresented, but atmospherically important, size regime.

Referring to the PTIR and Raman spectra also helps confirm whether a particle is a mixture, indicating that one particle has landed on another, which mimics the process of coagulation in the atmosphere. A mixed PS and SCR particle (structures in Figure 4a) is shown optically (Figure 4b), along with its PTIR and Raman spectra (Figure 4c,d). Sucrose can be identified by its C–H bend (δ_{CH}) at 1370 cm^{-1} in its PTIR spectrum, as well as 849 cm^{-1} in its Raman spectrum.⁵⁵ There are additional C–O stretches (ν_{CO}) in the fingerprint region for PTIR and Raman spectra, with the former spectrum containing stretches at 994 , 1044 , and 1130 cm^{-1} and the latter containing a stretching region at 1040 cm^{-1} . There are also strong indications of PS in both spectra; the PTIR spectrum has C–H stretches at 2846 and 2924 cm^{-1} , ring stretches at 1492 and 1602 cm^{-1} , and a C–H bend at 1452 cm^{-1} , whereas the Raman spectrum has C–H stretches at 2857 and 3058 cm^{-1} as well as ring stretches at 1008 and 1613 cm^{-1} . Utilizing CC-O-PTIR+Raman enables identification of MPs in multicomponent particles, which is critical for environmental samples.

It is acknowledged that many environmental MP particles do not resemble pristine plastics and may contain additional additives and fillers, products of ultraviolet (UV) photo-oxidation, and formation of biofilms.³ However, CC-O-PTIR+Raman has strong potential to identify characteristic peaks of MPs in these intricate spectra. For example, the carbonyl peaks resulting from photooxidation are readily distinguishable from many characteristic plastic peaks, such as C–H bends and stretches, although some of these peaks may be reduced over time with exposure to UV light.⁵⁶ As exemplified in Figure 4, the sharp peaks of plastics can be discerned when there is an overlap between organic peaks of different chemical species, and many ambient particle types also have broader peaks (Figure S8) than those found in pristine plastics.

The capability of CC-O-PTIR+Raman to distinguish MP particle types from ambient samples was further explored with the Ambient+MPs sample (Figure 5). All ambient particle types were placed together in one category (AMB) to simplify comparisons between the MP and non-MP particle types.

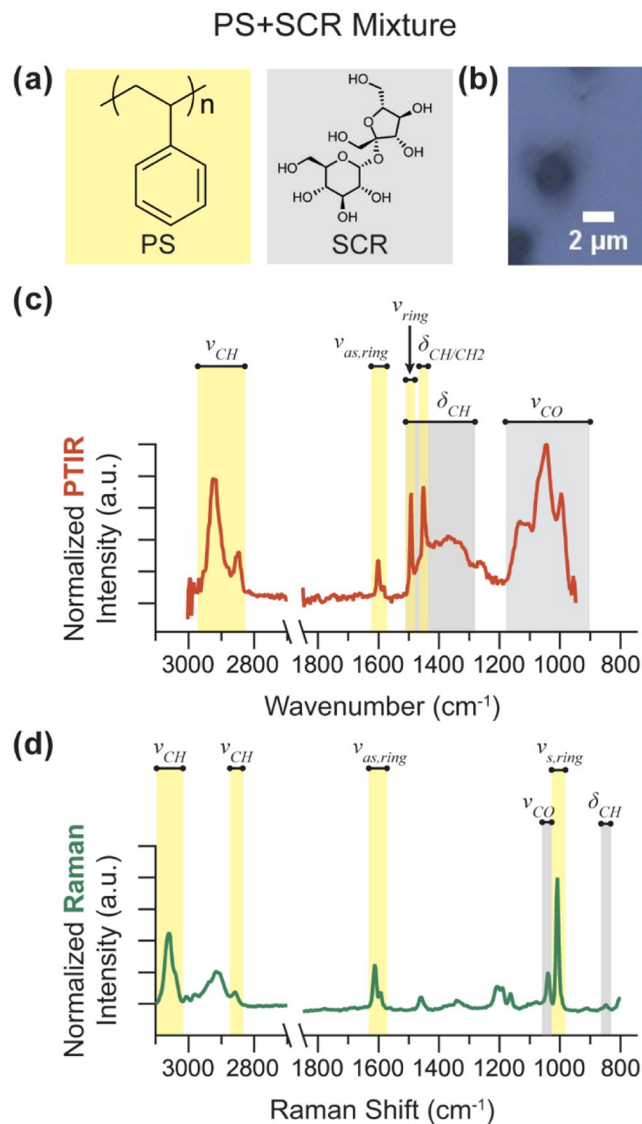


Figure 4. (a) Chemical structures of PS and SCR. (b) Optical image of a particle identified as a combination of PS and SCR (labeled MIX) as well as its (c) PTIR spectrum and (d) Raman spectrum. Peaks associated with PS and SCR are highlighted in yellow and gray, respectively.

Examples of the most common ambient particle types are shown in Figure S8. For the PTIR spectra, the AMB category had the largest fraction by far of 0.38 ± 0.08 . The fraction of Raman spectra labeled as AMB, in contrast, was 0.09 ± 0.05 , but fractions of spectra labeled as UNS or LOW for the technique cumulatively made up 0.5 ± 0.1 of all the particles in Figure 5a, primarily due to fluorescence or species with weak Raman signal. Previous studies have shown that fluorescence in Raman spectra is commonly encountered for ambient particles,^{37,38} so the increase in the UNS category is expected. Interestingly, the PTIR spectra had UNS and LOW fractions of 0.01 ± 0.01 and 0.05 ± 0.04 (Table S3), which was much lower than the fractions for the MPs-Only and MPs+Standards samples. The heat map in Figure 5b supports these observations as 52% of the time when the PTIR spectrum of a particle was labeled as AMB, its corresponding Raman spectrum was labeled as LOW, as shown in the gold box. This highlights a benefit of having information from O-PTIR. For

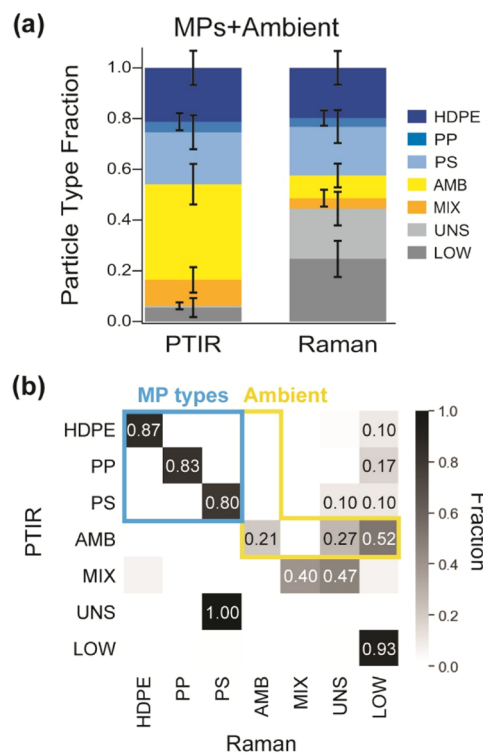


Figure 5. (a) Particle fractions from labeled PTIR and Raman spectra (particle count = 146). Error bars represent standard error for its respective particle type fraction. (b) A heat map of match fractions between the two groupings for each particle type (particle count = 262), with match fractions >0.10 labeled on their corresponding cells. MP and AMB cells are boxed in blue and gold, respectively, for clarity. In addition to the three MP particle types (e.g., HDPE, PP, and PS) as well as the MIX, UNS, and LOW categories, an ambient (AMB) category is also included.

the MP particle types, the PTIR and Raman spectra agreed $\geq 80\%$ of the time, indicating that the MPs were clearly distinguished from both ambient particles and from each other. This result shows that for ambient samples, O-PTIR has significant potential for particle characterization.

CONCLUSIONS

This study applied CC-O-PTIR+Raman for the first time to aerosolized MP particles, most of which were $\leq 5 \mu\text{m}$ in diameter, in samples of increasing complexity relevant to environmental, atmospheric studies. We show the capability of CC-O-PTIR+Raman to distinguish MP particle types from each other, as well as non-MP particle types. Reducing analysis time and labor with automation was a crucial improvement to the technique for collecting data sets large enough for quantitative analysis. However, spectral data sets will require methods that can label the unknown spectra with quantified statistical uncertainty,⁵⁷ preferably using both PTIR and Raman spectral inputs, since environmental studies often need to analyze large numbers of particles. We further demonstrate the application of CC-O-PTIR+Raman to identifying MPs in environmental matrices. The combination of PTIR and Raman spectra collected simultaneously leverages their respective strengths, including O-PTIR identification of ambient particles and Raman identification of pristine MPs. These complementary spectra will enable more reliable characterization of MPs that may have been mixed with

other environmental particles, and future studies can apply this technique to other MP particle morphologies (e.g., fibers) as well as environmental MPs. Although this newly automated technique was specifically applied to MP particles in this study, its benefits are widely applicable to characterization of atmospheric particles or other fields requiring IR and Raman analysis of particles $<10\text{ }\mu\text{m}$ in diameter.

■ ASSOCIATED CONTENT

Data Availability Statement

Associated images and data for all figures in the main text and *Supporting Information* are publicly available at University of Michigan – Deep Blue Data.⁵⁸

● Supporting Information

The Supporting Information is available free of charge at <https://pubs.acs.org/doi/10.1021/acs.analchem.5c02968>.

APS size distributions for laboratory-generated particle types and ambient particles collected, image of the PTIR Studios featurefindIR module, optical images of gridded silicon substrate used for the MPs+Ambient sample, particle fraction plots and values for all PTIR and Raman spectra, mIRage PTIR and Raman reference libraries, trends for all spectra labeled as LOW, matrix calculations used to make heat maps comparing PTIR and Raman spectra, and example ambient spectra of most common particle types seen in MPs+Ambient sample ([PDF](#))

■ AUTHOR INFORMATION

Corresponding Author

Andrew P. Ault — Department of Chemistry, University of Michigan, Ann Arbor, Michigan 48109, United States;
 orcid.org/0000-0002-7313-8559; Email: aulta@umich.edu

Authors

Rebecca L. Parham — Department of Chemistry, University of Michigan, Ann Arbor, Michigan 48109, United States;
 orcid.org/0000-0001-9513-4172

Abbygail M. Ayala — Department of Chemistry, University of Michigan, Ann Arbor, Michigan 48109, United States;
 orcid.org/0000-0002-1290-6788

Lauren Meagher — Department of Chemistry, University of Michigan, Ann Arbor, Michigan 48109, United States

Madelene E. Clough — Department of Chemistry, University of Michigan, Ann Arbor, Michigan 48109, United States;
 orcid.org/0000-0001-7534-4703

Eduardo Ochoa Rivera — Department of Statistics, University of Michigan, Ann Arbor, Michigan 48109, United States

Jia H. Shi — Department of Chemistry, University of Michigan, Ann Arbor, Michigan 48109, United States;  orcid.org/0000-0001-6319-8278

Ambuj Tewari — Department of Statistics and Department of Electrical Engineering and Computer Science, University of Michigan, Ann Arbor, Michigan 48109, United States;

 orcid.org/0000-0001-6969-7844

Anne J. McNeil — Department of Chemistry, University of Michigan, Ann Arbor, Michigan 48109, United States; Macromolecular Science and Engineering Program and Program in the Environment, University of Michigan, Ann Arbor, Michigan 48109, United States;  orcid.org/0000-0003-4591-3308

Complete contact information is available at:

<https://pubs.acs.org/10.1021/acs.analchem.5c02968>

Notes

The authors declare no competing financial interest.

■ ACKNOWLEDGMENTS

Primary funding was provided by the Meet the Moment initiative through the College of Literature, Science, and the Arts at the University of Michigan. R.L.P was funded in part by the National Science Foundation Graduate Research Fellowship Program (DGE-2241144). J.H.S. was supported in part by a University of Michigan Rackham Merit Fellowship. Sergey Zayats, Eoghan Dillon, and the Photothermal Spectroscopy Corp. team are gratefully acknowledged for instrument support.

■ REFERENCES

- (1) Jambeck, J. R.; Geyer, R.; Wilcox, C.; Siegler, T. R.; Perryman, M.; Andrady, A.; Narayan, R.; Law, K. L. *Science* **2015**, 347 (6223), 768–771.
- (2) Geyer, R.; Jambeck, J. R.; Law, K. L. *Sci. Adv.* **2017**, 3 (7), No. e1700782.
- (3) Hale, R. C.; Seeley, M. E.; La Guardia, M. J.; Mai, L.; Zeng, E. Y. *J. Geophys. Res.:Oceans* **2020**, 125 (1), 1–40.
- (4) Rochman, C. M.; Hoellein, T. *Science* **2020**, 368 (6496), 1184–1185.
- (5) Dris, R.; Gasperi, J.; Rocher, V.; Saad, M.; Renault, N.; Tassin, B. *Environ. Chem.* **2015**, 12 (5), 592–599.
- (6) Amato-Lourenço, L. F.; dos Santos Galvão, L.; Wiebeck, H.; Carvalho-Oliveira, R.; Mauad, T. *Sci. Total Environ.* **2022**, 821, No. 153450.
- (7) Cai, L.; Wang, J.; Peng, J.; Tan, Z.; Zhan, Z.; Tan, X.; Chen, Q. *Environ. Sci. Pollut. Res.* **2017**, 24 (32), 24928–24935.
- (8) Chen, Y.; Niu, J.; Xu, D.; Zhang, M.; Sun, K.; Gao, B. *Environ. Sci. Technol.* **2023**, 57 (30), 11152–11162.
- (9) Liu, K.; Wang, X.; Wei, N.; Song, Z.; Li, D. *Environ. Int.* **2019**, 132, No. 105127.
- (10) Thinh, T. Q.; Sang, T. T. N.; Viet, T. Q.; Tam, L. T. M.; Dan, D. P.; Strady, E.; Chung, K. L. T. *Vietnam J. Sci., Technol. Eng.* **2020**, 62 (3), 83–89.
- (11) Wright, S. L.; Ulke, J.; Font, A.; Chan, K. L. A.; Kelly, F. J. *Environ. Int.* **2020**, 136, No. 105411.
- (12) Brahney, J.; Hallerud, M.; Heim, E.; Hahnenberger, M.; Sukumaran, S. *Science* **2020**, 368 (6496), 1257–1260.
- (13) Bergmann, M.; Mützel, S.; Primpke, S.; Tekman, M. B.; Trachsel, J.; Gerdts, G. *Sci. Adv.* **2019**, 5 (8), No. eaax1157.
- (14) Allen, D.; Allen, S.; Abbasi, S.; Baker, A.; Bergmann, M.; Brahney, J.; Butler, T.; Duce, R. A.; Eckhardt, S.; Evangelou, N.; et al. *Nat. Rev. Earth Environ.* **2022**, 3 (6), 393–405.
- (15) Allen, S.; Allen, D.; Phoenix, V. R.; Le Roux, G.; Durández Jiménez, P.; Simonneau, A.; Binet, S.; Galop, D. *Nat. Geosci.* **2019**, 12 (5), 339–344.
- (16) Allen, S.; Allen, D.; Baladima, F.; Phoenix, V. R.; Thomas, J. L.; Le Roux, G.; Sonke, J. E. *Nat. Commun.* **2021**, 12 (1), No. 7242.
- (17) Liu, K.; Wu, T.; Wang, X.; Song, Z.; Zong, C.; Wei, N.; Li, D. *Environ. Sci. Technol.* **2019**, 53 (18), 10612–10619.
- (18) Zhang, Y.; Kang, S.; Allen, S.; Allen, D.; Gao, T.; Sillanpää, M. *Earth-Sci. Rev.* **2020**, 203, No. 103118.
- (19) Luo, X.; Wang, Z.; Yang, L.; Gao, T.; Zhang, Y. *Sci. Total Environ.* **2022**, 828, No. 154487.
- (20) Eberhard, T.; Casillas, G.; Zarus, G. M.; Barr, D. B. *J. Exposure Sci. Environ. Epidemiol.* **2024**, 34, 185–196.
- (21) Zhang, Y.; Slade, J. H.; Ault, A. P.; Chan, A. W. H. *Environ. Sci. Technol.* **2025**, 59 (16), 7810–7819.
- (22) Amato-Lourenço, L. F.; Carvalho-Oliveira, R.; Júnior, G. R.; dos Santos Galvão, L.; Ando, R. A.; Mauad, T. *J. Hazard. Mater.* **2021**, 416, No. 126124.

- (23) Jenner, L. C.; Rotchell, J. M.; Bennett, R. T.; Cowen, M.; Tentzeris, V.; Sadofsky, L. R. *Sci. Total Environ.* **2022**, *831*, No. 154907.
- (24) Boobis, A.; Cassee, F.; Gouin, T.; Koelmans, B.; Price, S.; Wagener, S.; Wright, S. 7. Summary and Research Topics. In *Dietary and Inhalation Exposure to Nano- and Microplastic Particles and Potential Implications for Human Health*; World Health Organization, 2022.
- (25) Adar, S. D.; Filigrana, P. A.; Clements, N.; Peel, J. L. *Curr. Environ. Health Rep.* **2014**, *1* (3), 258–274.
- (26) Brunekreef, B.; Forsberg, B. *Eur. Respir. J.* **2005**, *26* (2), 309–318.
- (27) Pope, C. A.; Ezzati, M.; Dockery Douglas, W. N. *Engl. J. Med.* **2009**, *360* (4), 376–386.
- (28) Pope, C. A.; Turner, M. C.; Burnett, R. T.; Jerrett, M.; Gapstur, S. M.; Diver, W. R.; Krewski, D.; Brook, R. D. *Circ. Res.* **2015**, *116* (1), 108–115.
- (29) Sacks, J.; Buckley, B.; Alexis, N.; Angrish, M.; Beardslee, R.; Benson, A.; Brown, J.; Buckley, B.; Campen, M.; Chan, E. et al. *Integrated Science Assessment (ISA) for Particulate Matter (Final Report, Dec 2019)*; EPA/600/R-19/188; U.S. Environmental Protection Agency: Washington, DC, 2019.
- (30) Dong, M.; She, Z.; Xiong, X.; Ouyang, G.; Luo, Z. *Anal. Bioanal. Chem.* **2022**, *414* (11), 3359–3372.
- (31) Käppler, A.; Fischer, D.; Oberbeckmann, S.; Schernewski, G.; Labrenz, M.; Eichhorn, K.-J.; Voit, B. *Anal. Bioanal. Chem.* **2016**, *408* (29), 8377–8391.
- (32) Löder, M. G. J.; Kuczera, M.; Mintenig, S.; Lorenz, C.; Gerdts, G. *Environ. Chem.* **2015**, *12* (5), 563–581.
- (33) Primpke, S.; Lorenz, C.; Rascher-Friesenhausen, R.; Gerdts, G. *Anal. Methods* **2017**, *9* (9), 1499–1511.
- (34) Käppler, A.; Windrich, F.; Löder, M. G. J.; Malanin, M.; Fischer, D.; Labrenz, M.; Eichhorn, K.-J.; Voit, B. *Anal. Bioanal. Chem.* **2015**, *407* (22), 6791–6801.
- (35) Levermore, J. M.; Smith, T. E. L.; Kelly, F. J.; Wright, S. L. *Anal. Chem.* **2020**, *92* (13), 8732–8740.
- (36) Wright, S. L.; Levermore, J. M.; Kelly, F. J. *Environ. Sci. Technol.* **2019**, *53* (15), 8947–8956.
- (37) Craig, R. L.; Bondy, A. L.; Ault, A. P. *Aerosol Sci. Technol.* **2017**, *51* (9), 1099–1112.
- (38) Doughty, D. C.; Hill, S. C. *J. Quant. Spectrosc. Radiat. Transfer* **2020**, *244*, No. 106839.
- (39) Böke, J. S.; Popp, J.; Krafft, C. *Sci. Rep.* **2022**, *12* (1), No. 18785.
- (40) Zhang, D.; Li, C.; Zhang, C.; Slipchenko, M. N.; Eakins, G.; Cheng, J.-X. *Sci. Adv.* **2016**, *2* (9), No. e1600521.
- (41) Olson, N. E.; Xiao, Y.; Lei, Z.; Ault, A. P. *Anal. Chem.* **2020**, *92* (14), 9932–9939.
- (42) Laskins, O.; Morris, H. S.; Grandquist, J. R.; Estillore, A. D.; Stone, E. A.; Grassian, V. H.; Tivanski, A. V. *Environ. Sci. Technol.* **2015**, *49* (22), 13447–13453.
- (43) Sublett, D. M., Jr.; Sendula, E.; Lamadrid, H.; Steele-MacInnis, M.; Spiekermann, G.; Burruss, R. C.; Bodnar, R. J. *J. Raman Spectrosc.* **2020**, *51* (3), 555–568.
- (44) Mirrieles, J. A.; Kirpes, R. M.; Haas, S. M.; Rauschenberg, C. D.; Matrai, P. A.; Remenapp, A.; Boschi, V. L.; Grannas, A. M.; Pratt, K. A.; Ault, A. P. *ACS Meas. Sci. Au* **2022**, *2* (6), 605–619.
- (45) Shi, J. H.; Poworoznek, C. J.; Parham, R. L.; Kolozsvari, K. R.; Olson, N. E.; Xiao, Y.; Lei, Z.; Birbeck, J. A.; Jacquemin, S. J.; Westrick, J. A.; Ault, A. P. *J. Phys. Chem. A* **2025**, *129* (5), 1429–1440.
- (46) Veerasingam, S.; Ranjani, M.; Venkatachalapathy, R.; Bagaev, A.; Mukhanov, V.; Litvinyuk, D.; Mugilarasan, M.; Gurumoorthi, K.; Guganathan, L.; Aboobacker, V. M.; Vethamony, P. *Crit. Rev. Environ. Sci. Technol.* **2021**, *51* (22), 2681–2743.
- (47) Taudul, B.; Tielens, F.; Calatayud, M. *J. Phys. Chem. B* **2024**, *128* (17), 4243–4254.
- (48) Nava, V.; Frezzotti, M. L.; Leoni, B. *Appl. Spectrosc.* **2021**, *75* (11), 1341–1357.
- (49) Bondy, A. L.; Bonanno, D.; Moffet, R. C.; Wang, B.; Laskin, A.; Ault, A. P. *Atmos. Chem. Phys.* **2018**, *18* (16), 12595–12612.
- (50) Ault, A. P.; Guasco, T. L.; Baltrusaitis, J.; Ryder, O. S.; Trueblood, J. V.; Collins, D. B.; Ruppel, M. J.; Cuadra-Rodriguez, L. A.; Prather, K. A.; Grassian, V. H. *J. Phys. Chem. Lett.* **2014**, *5*, 2493–2500.
- (51) Lei, Z.; Zhang, J.; Mueller, E. A.; Xiao, Y.; Kolozsvari, K. R.; McNeil, A. J.; Banaszak Holl, M. M.; Ault, A. P. *Anal. Chem.* **2022**, *94* (35), 11973–11977.
- (52) Shen, H. R.; Peters, T. M.; Casuccio, G. S.; Lersch, T. L.; West, R. R.; Kumar, A.; Kumar, N.; Ault, A. P. *Environ. Sci. Technol.* **2016**, *50* (10), 4961–4970.
- (53) Axson, J. L.; Shen, H. R.; Bondy, A. L.; Landry, C. C.; Welz, J.; Creamean, J. M.; Ault, A. P. *Aerosol Air Qual. Res.* **2016**, *16* (3), 555–567.
- (54) Ault, A. P.; Axson, J. L. *Anal. Chem.* **2017**, *89* (1), 430–452.
- (55) Brizuela, A. B.; Bichara, L. C.; Romano, E.; Yurquina, A.; Locatelli, S.; Brandán, S. A. *Carbohydr. Res.* **2012**, *361*, 212–218.
- (56) Nwachukwu, O.; Kniazev, K.; Abarca Perez, A.; Kuno, M.; Doudrick, K. *Environ. Sci. Technol.* **2024**, *58* (2), 1312–1320.
- (57) Clough, M. E.; Ochoa Rivera, E.; Parham, R. L.; Ault, A. P.; Zimmerman, P. M.; McNeil, A. J.; Tewari, A. *Environ. Sci. Technol.* **2024**, *58* (49), 21740–21749.
- (58) Parham, R. L.; Ayala, A. M.; Meagher, L.; Clough, M. E.; Ochoa Rivera, E.; Shi, J. H.; Tewari, A.; McNeil, A. J.; Ault, A. P. Dataset for Identifying Aerosolized Microplastics, Standards, and Ambient Particles with Photothermal Infrared and Raman Spectra. University of Michigan - Deep Blue Data: Ann Arbor, MI, 2025.

CAS BIOFINDER DISCOVERY PLATFORM™

ELIMINATE DATA SILOS. FIND WHAT YOU NEED, WHEN YOU NEED IT.

A single platform for relevant, high-quality biological and toxicology research

Streamline your R&D

CAS A division of the American Chemical Society